Target-based coherent beam combining of an optical phased array fed by a broadband laser source

Milo W. Hyde IV, Jack E. McCrae & Glenn A. Tyler

Published online: 18 Jul 2017.

Submit your article to this journal ↗

View related articles ↗

View Crossmark data ↗

Taylor & Francis
Taylor & Francis Group

Check for updates

Target-based coherent beam combining of an optical phased array fed by a broadband laser source

Milo W. Hyde IV[a], Jack E. McCrae[b] and Glenn A. Tyler[c]

[a]Department of Electrical and Computer Engineering, Air Force Institute of Technology, Dayton, OH, USA; [b]Department of Engineering Physics, Air Force Institute of Technology, Dayton, OH, USA; [c]The Optical Sciences Company, Anaheim, CA, USA

ABSTRACT

The target-based phasing of an optical phased array (OPA) fed by a broadband master oscillator laser source is investigated. The specific scenario examined here considers an OPA phasing through atmospheric turbulence on a rough curved object. An analytical expression for the detected or received intensity is derived. Gleaned from this expression are the conditions under which target-based phasing is possible. A detailed OPA wave optics simulation is performed to validate the theoretical findings. Key aspects of the simulation set-up as well as the results are thoroughly discussed.

1. Introduction

The desire to create lightweight, conformal high-energy laser systems has motivated the development of optical phased array (OPA) technologies – most notably, fibre laser technology and active phase locking schemes, e.g. locking of optical coherence by single-detector electronic-frequency tagging (LOCSET) (1–3) and stochastic parallel gradient descent (SPGD) (1, 4, 5). An obvious requirement of actively phase-locked, or coherently combined fibre laser systems is that the optical path length differences (OPDs) of the fibres feeding the OPA elements be much smaller than the coherence length $l_c = c\tau_c$, where c is the speed of light in vacuum and τ_c is the coherence time of the master oscillator (MO) laser source. This prompts the use of narrowband MOs when constructing OPAs, which works quite well for coherently combining arrays of low-power fibre lasers.

The desire for higher and higher output powers brings nonlinear optical effects – stimulated Brillouin scattering (SBS) being the dominant mechanism – into play (1, 6). The most common technique for suppressing SBS, i.e. reduce the SBS gain or raise the SBS threshold, is to broaden the MO's bandwidth (typically, to values greater than 10 GHz) (6). Thus, the OPDs of the fibres feeding the array elements must be submillimeter for active coherent beam combining (CBC) to work effectively.

Although this path length matching requirement is a challenge, CBC of fibre lasers fed by artificially-broadened MOs has been successfully demonstrated (1, 7–10). All of these works phased the array locally.

Creating a lightweight, conformal OPA weapon requires target-based phasing, where target shape and the environment (predominately, atmospheric turbulence) need to be considered.

In addition to the requirement that any target-induced phase be estimated and rejected (11), target shape can affect target-based CBC systems in a more fundamental way. Consider a locally phased OPA fed by a broadband MO propagating through turbulence and illuminating a target with many scattering features. If these target features are separated by less than $l_c/2$, phasing the array on the target should clearly be possible. Indeed, this was recently demonstrated experimentally (12).

If, on the other hand, the dominant scattering features are separated by more than $l_c/2$ (the more likely scenario, considering $l_c/2 < 5$ mm), the light scattered from each feature adds incoherently back in the array's receiver or detector plane. All active CBC systems, whether phasing locally or on a distant object, must detect a change in the received intensity in order to phase. This changing intensity is due to the phase modulations or dithers placed on each array beam. It stands to reason that if the received intensity contains many contributions from the target which add incoherently, the effect of the modulations or dithers on the received intensity could be lost and subsequently, target-based phasing could fail.

Only recently has this problem been investigated (13–15). In (13, 14), it was found that target-based phasing was possible, even on a target with scattering features separated by many l_c, if the received intensity changed

---

with the modulations or dithers of the array. This implies that the field incident on the target must also change with the element dithers, which is another way of stating that coherent light must be incident on the target. These works did not consider atmospheric turbulence or target-induced speckle and considered only simple targets – a mirror, step pyramid and parabolic target in the former and a simple step target in the latter. Reference (*15*) extended (*14*) by including turbulence and speckle, but again, only considered a step target.

In this paper, the effect a linewidth-broadened MO has on target-based phasing is investigated further. Here, atmospheric turbulence and a rough parabolic target, with a depth much greater than l_c, are considered. Section 2 examines the scenario analytically. An expression for the received intensity is derived and the conditions under which target-based phasing is possible are discussed. Lastly, to validate the theoretical findings, Section 3 presents simulation results of a seven element hexagonal array, fed by a 25 GHz white-noise-broadened MO (*9*), phasing through turbulence on a rough parabolic target. Key aspects of the simulation set-up as well as a thorough discussion of the results are provided.

2. Theory

The relevant geometry is shown in Figure 1. Light from a MO laser source passes through an electro-optical modulator (EOM), which artificially broadens the MO's linewidth, before being split into N fibres. The light in each fibre passes through an EOM and amplifier before being expanded and collimated by a beam expander or telescope. The EOMs apply phase modulations or dithers – either random or sinusoidal (e.g. SPGD or LOCSET) – to the light in the fibres.

The light leaves the N element array and is focused through atmospheric turbulence on an optically rough parabolic target located at $z = L$. The parabolic target has a base diameter D_T, radius of curvature R_T and rough surface profile $h(\rho)$.

The light scattered from the target propagates back through the same atmospheric turbulence before being measured by detectors in the array plane at $z = 0$. The signals from the detectors are 'demodulated' in some fashion to yield estimates for the transmitter and atmospheric phases. Using the EOMs, the conjugates of these phases are then applied to the transmitters, correcting the telescope and atmospheric aberrations and phasing the array on the target.

In the theoretical analysis to follow, turbulence and target roughness are omitted. Atmospheric turbulence and speckle are included in the simulation discussed in Section 3.

The array plane field takes the form

$$U^{\mathrm{ar}}(\boldsymbol{\rho}, t) = \sum_{n=1}^{N} \frac{A_n}{N} \mathcal{L}\left[t - \frac{\varepsilon_n(t)}{c} + \frac{C_n(t)}{c} - \frac{B_n(t)}{c}\right]$$
$$\times \operatorname{circ}\left(\frac{|\boldsymbol{\rho} - \boldsymbol{\rho}_n|}{d/2}\right), \quad (1)$$

where $\operatorname{circ}(x)$ is the circle function defined by Goodman (*16*), d is the diameter of a transmitter, $\boldsymbol{\rho} = \hat{x}x + \hat{y}y$, and $\boldsymbol{\rho}_n = \hat{x}x_n + \hat{y}y_n$ is a vector that points from the origin to the nth transmitter or beam centre. The A_n/N term combines the effects of the fibre splitter and amplifier. The functions $\varepsilon_n(t)$, $C_n(t)$ and $B_n(t)$ represent the path length error, correction, and modulation for the nth beam, respectively. ε/c physically model the combined temporal delays introduced by the amplifiers as well as the fibres feeding the transmitters. They are assumed to vary much more slowly than the beam modulations B and corrections C. Lastly, $\mathcal{L}$ is the random laser field and is assumed to be a sample function drawn from a wide-sense stationary (WSS) random process.

Using the Fourier transform pair (*17*, *18*),

$$f(\omega) = \frac{1}{2\pi} \int_{-\infty}^{\infty} f(t) e^{j\omega t} \mathrm{d}t$$
$$f(t) = \int_{-\infty}^{\infty} f(\omega) e^{-j\omega t} \mathrm{d}\omega \quad (2)$$

and assuming that the Fourier transform of $\mathcal{L}$ exists, the array plane field becomes

$$U^{\mathrm{ar}}(\boldsymbol{\rho}, \omega) = \sum_{n=1}^{N} \frac{A_n}{N} \mathcal{L}_n(\omega) \operatorname{circ}\left(\frac{|\boldsymbol{\rho} - \boldsymbol{\rho}_n|}{d/2}\right). \quad (3)$$

The field in the target plane is found using the Fresnel propagation integral (*16*) (recall that the array field is focused on the target):

$$U^{\mathrm{tar}}(\boldsymbol{\rho}, L, \omega) = \frac{e^{jkL} e^{\frac{jk}{2L}\rho^2}}{j\lambda L} \sum_{n=1}^{N} \frac{A_n}{N} \mathcal{L}_n(\omega) \pi \left(\frac{d}{2}\right)^2$$
$$\times \operatorname{jinc}\left(\frac{k}{L}\frac{d}{2}\rho\right) \exp{-j\frac{k}{L}\boldsymbol{\rho} \cdot \boldsymbol{\rho}_n}, \quad (4)$$

where λ is the wavelength, $k = 2\pi/\lambda$ is the wavenumber, and $\operatorname{jinc}(x) = 2J_1(x)/x$ (*16*).

The field scattered from the parabolic target is approximately

$$U^{\mathrm{scat}}(\boldsymbol{\rho}, L, \omega) \approx \operatorname{circ}\left(\frac{\rho}{D_T/2}\right) \exp\left(\frac{j2k}{2R_T}\rho^2\right)$$
$$\times U^{\mathrm{tar}}(\boldsymbol{\rho}, L, \omega). \quad (5)$$
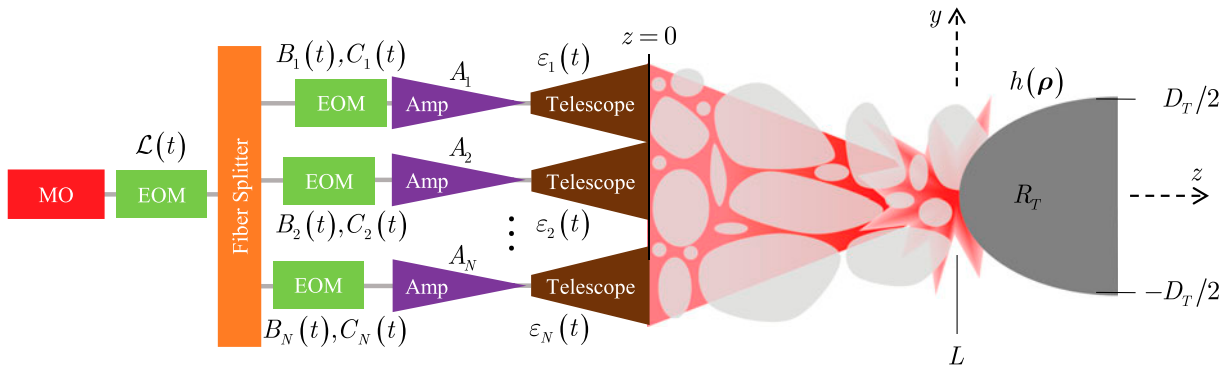
Figure 1. N element fibre laser array geometry – MO is master oscillator, EOM is electro-optical modulator, and Amp is amplifier.

With this expression, the field scattered back to the array plane (the received field) can be found by again, employing the Fresnel propagation integral:

$$
U^{\text{rec}}(\boldsymbol{\rho}, 0, \omega)
$$

$$
= \frac{e^{j2kL} e^{\frac{jk}{2L}\rho^2}}{j\lambda L} \frac{\pi (d/2)^2}{j\lambda L}
$$

$$
\times \sum_{n=1}^{N} \frac{A_n}{N} \mathcal{L}_n(\omega) \iint_{-\infty}^{\infty} \text{circ}\left(\frac{\rho'}{D_T/2}\right) \text{jinc}\left(\frac{k}{L}\frac{d}{2}\rho'\right)
$$

$$
\times \exp\left\{jk\left[\left(\frac{1}{R_T}+\frac{1}{L}\right)\rho'^2 - \frac{\boldsymbol{\rho}+\boldsymbol{\rho}_n}{L}\cdot\boldsymbol{\rho}'\right]\right\} d^2\rho'.
\tag{6}
$$

The above integrals cannot be evaluated analytically; however, an approximate result can be obtained using the method of stationary phase (MoSP) (*17*). The accuracy of the MoSP approximation improves as $R_T \to 0$ and is quite good for values of $R_T < 0.1L$. Applying the MoSP, neglecting the end-point contributions (i.e. critical points of the second kind) from the circ function, and simplifying yields

$$
U^{\text{rec}}(\boldsymbol{\rho}, 0, \omega)
$$

$$
\approx \frac{1}{2(1+L/R_T)} \sum_{n=1}^{N} \frac{A_n}{N}
$$

$$
\times \left[\frac{\pi (d/2)^2}{j\lambda L} \text{jinc}\left(\frac{k}{L}\frac{d}{2}\frac{|\boldsymbol{\rho}+\boldsymbol{\rho}_n|}{2(1+L/R_T)}\right)\right]
$$

$$
\times \mathcal{L}_n(\omega) \exp\left\{jk\left[2L+\frac{\rho^2}{2L}-\frac{|\boldsymbol{\rho}+\boldsymbol{\rho}_n|^2}{2L(1+L/R_T)}\right]\right\}.
\tag{7}
$$

The received field in the time domain can be found by inverse Fourier transforming (7). This process is made simpler by assuming that the laser's bandwidth is much less than the mean laser frequency, i.e. $\Delta\omega \ll \bar{\omega}$. This

assumption permits the bracketed quantity containing the jinc function to be evaluated at $\bar{\omega}$ and the inverse Fourier transform to be performed on the remaining terms:

$$
U^{\text{rec}}(\boldsymbol{\rho}, 0, t)
$$

$$
\approx \frac{1}{2(1+L/R_T)} \sum_{n=1}^{N} \frac{A_n}{N}
$$

$$
\times \left[\frac{\pi (d/2)^2}{j\bar{\lambda}L} \text{jinc}\left(\frac{\bar{k}}{L}\frac{d}{2}\frac{|\boldsymbol{\rho}+\boldsymbol{\rho}_n|}{2(1+L/R_T)}\right)\right]
$$

$$
\times \mathcal{L}\left[t-t_n-\Phi_n(t-t_n)\right],
\tag{8}
$$

where

$$
t_n = \frac{2L}{c}+\frac{\rho^2}{2Lc}-\frac{|\boldsymbol{\rho}+\boldsymbol{\rho}_n|^2}{2Lc(1+L/R_T)}
$$

$$
\Phi_n(t) = \frac{\varepsilon_n(t)}{c}-\frac{C_n(t)}{c}+\frac{B_n(t)}{c}.
\tag{9}
$$

The detector signals, from which the path length errors ε are estimated, are proportional to the received intensity, namely

$$
I^{\text{rec}}(\boldsymbol{\rho}, t) = \left\langle \left|U^{\text{rec}}(\boldsymbol{\rho}, 0, t)\right|^2 \right\rangle
$$

$$
= \frac{1}{4(1+L/R_T)^2} \sum_{n=1}^{N}\sum_{m=1}^{N} \frac{A_n A_m}{N^2} \left[\frac{\pi (d/2)^2}{\bar{\lambda}L}\right]^2
$$

$$
\times \text{jinc}\left(\frac{\bar{k}}{L}\frac{d}{2}\frac{|\boldsymbol{\rho}+\boldsymbol{\rho}_n|}{2(1+L/R_T)}\right) \text{jinc}\left(\frac{\bar{k}}{L}\frac{d}{2}\frac{|\boldsymbol{\rho}+\boldsymbol{\rho}_m|}{2(1+L/R_T)}\right)
$$

$$
\times \left\langle \mathcal{L}\left[t-t_n-\Phi_n(t-t_n)\right]\mathcal{L}^*\left[t-t_m-\Phi_m(t-t_m)\right]\right\rangle,
\tag{10}
$$

where the averaging is performed over the ensemble of U^{rec} realizations. Recall that $\mathcal{L}$ is assumed to be WSS and

therefore,

$$\langle \mathcal{L}(t_1) \mathcal{L}^*(t_2) \rangle = I^{\text{MO}} \gamma (t_1 - t_2), \qquad (11)$$

where I^{MO} is the MO's average intensity and γ is the complex degree of temporal coherence [i.e. the complex degree of self coherence in Goodman's terminology (18)]. Substituting (11) into (10) produces the desired result:

$$
\begin{aligned}
I^{\text{rec}}(\boldsymbol{\rho}, t) &= \frac{I^{\text{MO}}}{4\left(1 + L/R_T\right)^2} \sum_{n=1}^{N} \sum_{m=1}^{N} \frac{A_n A_m}{N^2} \\
&\times \left[\frac{\pi \left(d/2\right)^2}{\bar{\lambda} L}\right]^2 \text{jinc}\left(\frac{\bar{k}}{L} \frac{d}{2} \frac{|\boldsymbol{\rho} + \boldsymbol{\rho}_n|}{2\left(1 + L/R_T\right)}\right) \\
&\times \text{jinc}\left(\frac{\bar{k}}{L} \frac{d}{2} \frac{|\boldsymbol{\rho} + \boldsymbol{\rho}_m|}{2\left(1 + L/R_T\right)}\right) \\
&\times \gamma \left[t_m + \Phi_m \left(t - t_m\right) - t_n - \Phi_n \left(t - t_n\right)\right].
\end{aligned}
\qquad (12)
$$

Note that although $\mathcal{L}$ is assumed to be WSS, the resulting random field U^{rec} is not.

The above expression is the key analytical result of this paper and warrants further discussion. The $n = m$ terms of the double summation yield the incoherent intensity; the $n \neq m$ terms yield the coherent intensity. Since they contain the path length errors ε, corrections C and modulations B, the coherent terms must be detected to successfully phase the array on the target. Detection of these terms requires that $|\gamma| > 0$ for all n and m – how much greater depends on the noise level.

Thus, the value of $t_m + \Phi_m \left(t - t_m\right) - t_n - \Phi_n \left(t - t_n\right)$ is of critical importance:

$$
\begin{aligned}
&t_m + \Phi_m \left(t - t_m\right) - t_n - \Phi_n \left(t - t_n\right) \\
&= \frac{\boldsymbol{\rho}_n - \boldsymbol{\rho}_m}{Lc\left(1 + L/R_T\right)} \cdot \boldsymbol{\rho} + \frac{\rho_n^2 - \rho_m^2}{2Lc\left(1 + L/R_T\right)} \\
&\quad + \frac{\varepsilon_m \left(t - t_m\right) - \varepsilon_n \left(t - t_n\right)}{c} \\
&\quad + \frac{C_n \left(t - t_n\right) - C_m \left(t - t_m\right)}{c} \\
&\quad + \frac{B_m \left(t - t_m\right) - B_n \left(t - t_n\right)}{c}.
\end{aligned}
\qquad (13)
$$

Consider first the arguments of ε, C, and B. The t_n, given in (9), are 'time-of-flight' delays and by far the dominant term is $2L/c$, i.e. the light travel time to the target and back. Thus, $t_n \approx 2L/c$ in ε, C, and B.

For $|\gamma|$, the remaining terms in (13) are negligible both going like $1/\left(cL^2\right)$, which is an extremely small number for any $L > 1$. In addition, the path length corrections C and modulations B are generally less than $\bar{\lambda}$ and can also be neglected. The $|\gamma|$ becomes

$$
\begin{aligned}
&\left|\gamma \left[t_m + \Phi_m \left(t - t_m\right) - t_n - \Phi_n \left(t - t_n\right)\right]\right| \\
&\approx \left|\gamma \left[\frac{\varepsilon_m \left(t - 2L/c\right) - \varepsilon_n \left(t - 2L/c\right)}{c}\right]\right|.
\end{aligned}
\qquad (14)
$$

This result is quite intuitive and states that in order to successfully phase on the target, the initial array path length errors (or OPDs) must be significantly less than the coherence length l_c. Although this result was derived assuming a parabolic target, it is quite clear that this condition must be met for any target-based OPA system regardless of target shape. Achieving this level of path length matching precision – for GHz bandwidths, submillimeter precision is required – will likely require a local phasing system in addition to the target-based system (1, 7, 9, 19). Note that the presence of atmospheric turbulence and a rough speckle target will not change this result. Atmospheric turbulence and surface roughness will generally introduce path length differences between the array beams of tens of $\bar{\lambda}$. For millimetre l_c, these OPDs are insignificant. Atmospheric turbulence and surface roughness are included in the simulation results presented in Section 3.

For $\arg(\gamma)$, at a minimum, the first term in (13), ε, C and B must be retained. The first term in (13) is the array factor (20). When the array is properly phased, it produces the narrow, high-intensity spot characteristic of coherently-combined laser array systems. In $\arg(\gamma)$, the path length errors ε, corrections C and modulations B appear as phase shifts which distort the desired, perfect array intensity pattern. In the case of ε, the distortion is unintentional. On the other hand, the B distortion is intentional and used to estimate and ultimately correct (with C) ε.

Considering the findings in the previous two paragraphs, the received intensity in (12) can be expressed in a more physical form:

$$
\begin{aligned}
I^{\text{rec}}(\boldsymbol{\rho}, t) &= I^{\text{rec,icoh}}(\boldsymbol{\rho}) + I^{\text{rec,coh}}(\boldsymbol{\rho}, t) \\
I^{\text{rec,icoh}}(\boldsymbol{\rho}) &\approx \frac{I^{\text{MO}}}{4\left(1 + L/R_T\right)^2} \sum_{n=1}^{N} \frac{A_n^2}{N^2} \left[\frac{\pi \left(d/2\right)^2}{\bar{\lambda} L}\right]^2 \\
&\times \text{jinc}^2\left(\frac{\bar{k}}{L} \frac{d}{2} \frac{|\boldsymbol{\rho} + \boldsymbol{\rho}_n|}{2\left(1 + L/R_T\right)}\right) \\
I^{\text{rec,coh}}(\boldsymbol{\rho}, t) &\approx \frac{I^{\text{MO}}}{4\left(1 + L/R_T\right)^2} \sum_{n=1}^{N} \sum_{m \neq n}^{N} \frac{A_n A_m}{N^2} \\
&\times \left[\frac{\pi \left(d/2\right)^2}{\bar{\lambda} L}\right]^2 \text{jinc}\left(\frac{\bar{k}}{L} \frac{d}{2} \frac{|\boldsymbol{\rho} + \boldsymbol{\rho}_n|}{2\left(1 + L/R_T\right)}\right) \\
&\times \text{jinc}\left(\frac{\bar{k}}{L} \frac{d}{2} \frac{|\boldsymbol{\rho} + \boldsymbol{\rho}_m|}{2\left(1 + L/R_T\right)}\right)
\end{aligned}
$$
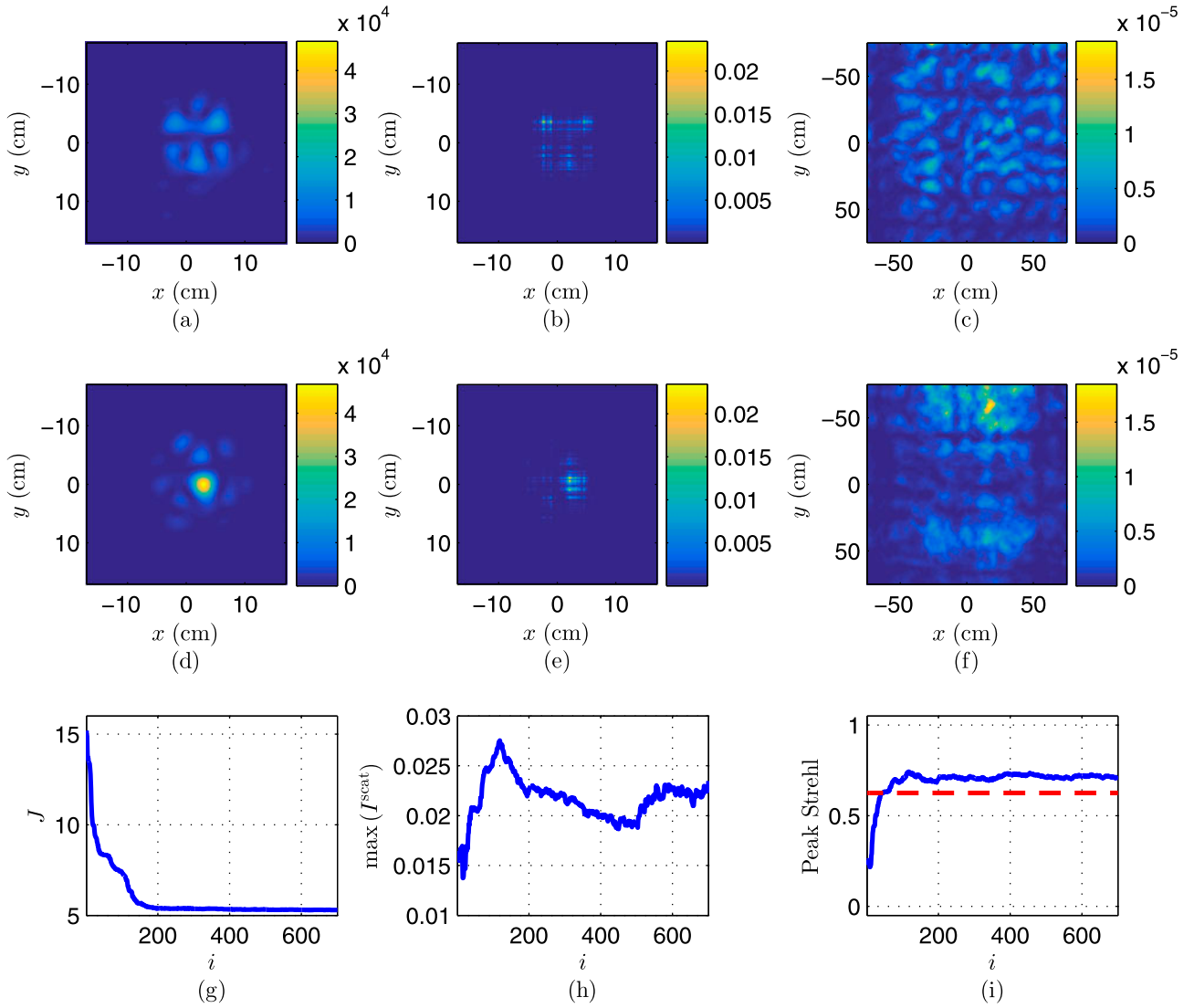
Figure 2. (a) I^{tar} on first SPGD iteration, (b) I^{scat} on first SPGD iteration, (c) I^{rec} on first SPGD iteration, (d) I^{tar} on 700th SPGD iteration, (e) I^{scat} on 700th SPGD iteration, (f) I^{rec} on 700th SPGD iteration, (g) objective function value J vs. iteration number i, (h) maximum of I^{scat} vs. iteration number i, and (i) target plane peak Strehl ratio vs. iteration number i.

$$\times \left| \gamma \left[\frac{\varepsilon_m \left(t - 2L/c \right) - \varepsilon_n \left(t - 2L/c \right)}{c} \right] \right|$$

$$\times \cos \left(\arg \left\{ \gamma \left[\frac{\boldsymbol{\rho}_n - \boldsymbol{\rho}_m}{Lc \left(1 + L/R_T \right)} \cdot \boldsymbol{\rho} \right. \right. \right.$$

$$+ \frac{\varepsilon_m \left(t - 2L/c \right) - \varepsilon_n \left(t - 2L/c \right)}{c}$$

$$+ \frac{C_n \left(t - 2L/c \right) - C_m \left(t - 2L/c \right)}{c}$$

$$\left. \left. \left. + \frac{B_m \left(t - 2L/c \right) - B_n \left(t - 2L/c \right)}{c} \right] \right\} \right), \qquad (15)$$

where $I^{\text{rec,icoh}}$ and $I^{\text{rec,coh}}$ are the incoherent and coherent intensities, respectively.

3. Validation

In this section, simulation results of an OPA phasing through atmospheric turbulence on a distant, rough, parabolic target are presented to complete the analysis presented above. Before presenting the results, key aspects of the simulation are discussed.

The simulated array was a seven-element array with circular transmitters arranged in a regular hexagon. The array transmitters each had an $A_n = \sqrt{1000}$, a diameter $d = 12.5$ cm and were centre-to-centre spaced $D = 13.1$ cm apart. The array, target and receiver planes were discretized using 1700 points per side with 2, 2.8 and 2 mm sample spacings, respectively.

To simulate white noise broadening (9), the MO's line shape was Gaussian with a $\Delta \nu = \Delta \omega / \left(2\pi \right) = 25$ GHz

full-width-at-half-maximum bandwidth and a mean frequency of $\bar{\nu} = 281.8$ THz ($\bar{\lambda} = 1.064$ μm). The coherence time and coherence length of the MO were $\tau_c = 26.6$ ps and $l_c = 8$ mm, respectively ([18]). The array path length errors ε were drawn from a zero-mean, $(l_c/10)^2$-variance normal distribution $[\varepsilon \sim \mathcal{N}(0, l_c^2/100)]$ using a Gaussian random number generator.

The spectral slicing method was used to simulate the finite temporal coherence of the MO ([21], [22]). Forty-five evenly spaced frequencies ν from $\bar{\nu} - 2\Delta\nu$ to $\bar{\nu} + 2\Delta\nu$ were used to discretize the Gaussian power spectral density ([18]), i.e.

$$\mathcal{G}(\nu) = \frac{2\sqrt{\ln 2}}{\sqrt{\pi}\,\Delta\nu} \exp\left[-\left(2\sqrt{\ln 2}\frac{\nu - \bar{\nu}}{\Delta\nu}\right)\right], \quad (16)$$

of the source.

The rough parabolic target, located $L = 10$ km away from the array, had a base diameter of $D_T = 1$ m and a radius of curvature of $R_T = 0.5$ m. The target's random surface heights were Gaussian distributed and Gaussian correlated with a standard deviation of $\sigma_h = 3\mu$m and spatial correlation length of $l_h = 60$ μm.

To prevent aliasing the received field, a Fresnel-filtered version of the target was used in the simulation, namely

$$T^{\mathrm{F}}(\boldsymbol{\rho}, \omega) = \frac{\exp\left(\frac{-\mathrm{j}k}{2L}\rho^2\right)}{(\lambda L)^2} \iint_{-\infty}^{\infty} \left\{ \mathrm{circ}\left(\frac{\rho'}{D_T/2}\right) \right.$$
$$\times \exp\left(\frac{\mathrm{j}2k}{2R_T}\rho'^2\right) \exp\left[\mathrm{j}2kh(\boldsymbol{\rho}')\right]\right\}$$
$$\times \exp\left(\frac{\mathrm{j}k}{2L}\rho'^2\right) \tilde{W}\left(\frac{\boldsymbol{\rho}' - \boldsymbol{\rho}}{\lambda L}\right) \mathrm{d}^2\rho', \quad (17)$$

where the quantity in the braces is the target T and $\tilde{W}$ is the Fourier transform of the window function W in the receiver plane. Here, W was a square with a side length D_W equal to 3/4 the size of the full computational grid, i.e. $D_W = 2.55$ m.

Adequately sampling T (in particular, T's phase curvature) to compute T^{F} requires 3.8 million points per side with a grid spacing of $0.25\bar{\lambda}$ ([23]). Using this number of points on 2D grids is impractical; however, computation and storage of Mega-point 1D grids is easily accomplished. Thus, (17) was approximated as

$$T^{\mathrm{F}}(\boldsymbol{\rho}, \omega) \approx T^{\mathrm{F}}(x, \omega) T^{\mathrm{F}}(y, \omega)$$
$$T^{\mathrm{F}}(\alpha, \omega) \approx \frac{\exp\left(\frac{-\mathrm{j}k}{2L}\alpha^2\right)}{\lambda L} \int_{-\infty}^{\infty} \mathrm{rect}\left(\frac{\alpha'}{D_T}\right)$$
$$\times \exp\left\{\mathrm{j}k\left[\left(\frac{1}{R_T} + \frac{1}{2L}\right)\alpha'^2 + 2h(\alpha')\right]\right\}$$

$$\times D_W \, \mathrm{sinc}\left[\frac{k}{L}\frac{D_W}{2}(\alpha' - \alpha)\right] \mathrm{d}\alpha', \quad (18)$$

where $\alpha = x, y$, rect (x) is the rectangle function defined by Goodman ([16]), and sinc $(x) = \sin(x)/x$.

Synthesis of T was as follows:

(1) Two independent 1D rough surface instances were generated using the Monte Carlo spectral method described in ([24]).
(2) Using the requisite number of points and grid spacing ([23]), the integral in (18) was computed numerically for each 1D rough surface instance.
(3) The x and y T^{F} were interpolated to the target plane grid dimensions stated above, i.e. 1700 points with a 2.8 mm spacing.
(4) The interpolated x and y T^{F} were expanded to 2D grids.
(5) $T^{\mathrm{F}}(\boldsymbol{\rho}) \approx T^{\mathrm{F}}(x) T^{\mathrm{F}}(y)$.

Steps 2–5 were repeated for each of the 45 ν making up the bandwidth of the source.

SPGD ([1], [4], [5]) was used to minimize the objective function $J = 1/l_s$, where l_s was the estimated width of the spatial autocovariance of I^{rec}. The spatial autocovariance of I^{rec} was computed over a square area, 1.5 m on a side. Note that l_s is physically the mean speckle width. It is well known that l_s is inversely related to the size of the spot on the target ([25]), thus, minimizing J minimizes the target spot which occurs when the array is properly phased. The SPGD dithers B applied to the transmitters were ± 53.2 nm (or $\pi/10$ at $\bar{\lambda}$), where the directions of the dithers were chosen at random with an equal probability of being positive or negative.

The atmospheric turbulence was simulated using four Kolmogorov phase screens evenly spaced along the $L = 10$ km path. Each phase screen was divided by $\bar{k}$ to convert to metres of optical path length. The turbulence was static over the duration of the simulation. The spherical wave Fried parameter and Rytov number of the turbulent path at $\bar{\lambda}$ were $r_{0,\mathrm{sw}} = 20.5$ cm and $\sigma_{\chi,\mathrm{sw}}^2 = 0.0512$, respectively.

The simulation was performed as follows:

(1) For each of the 45 ν,
  (a) The seven transmitter fields were individually propagated through the atmospheric turbulence to the target plane.
  (b) T^{F}, using the procedure detailed above, was computed and applied to each incident field to form the scattered fields
  (c) The seven scattered fields were individually propagated back through the same atmospheric

turbulence to the array plane producing the received fields.

(2) On each simulated SPGD iteration i or time step,

   (a) The SPGD fields were formed by summing the seven received fields with the appropriate dithers $B_{n,i}$, errors ε_n, and corrections $C_{n,i}$ for each of the 45 ν.

   (b) The received intensity I_i^{rec} was obtained by computing

$$I_i^{\text{rec}}(\boldsymbol{\rho}) = \int_{-\infty}^{\infty} \mathcal{G}(\nu)\left|U_i^{\text{rec}}(\boldsymbol{\rho},\nu)\right|^2 \, d\nu, \tag{19}$$

where $\mathcal{G}$ is given in (16), numerically over the 45 simulated ν using the trapezoidal method.

   (c) The objective function $J = 1/l_s$, where l_s was determined from the spatial autocovariance of I_i^{rec}, was computed.

   (d) The SPGD phase corrections were found using

$$C_{n,i+1} = C_{n,i} + \beta \delta J B_{n,i}, \tag{20}$$

where $\beta = -2$ was the gain and δJ was the change in the objective function.

(3) The simulation was halted after 700 SPGD iterations.

All propagations, from the array plane to the target plane and from the target plane back to the receiver plane, were computed using fast Fourier transforms.

Note that by performing the simulation in the manner outlined above, it is assumed that the received field U^{rec} is WSS over an SPGD iteration or time step. This is a valid approximation considering that an SPGD time step (roughly 1 μs) is much greater than $\tau_c = 26.6$ ps – nearly 38,000 independent realizations of I^{rec} are integrated on each SPGD iteration.

Figure 2 shows the simulation results: Figure 2(a)–(c) shows the target plane intensity I^{tar}, scattered intensity I^{scat} and I^{rec} on the first SPGD iteration, respectively. Figure 2(d)–(f) show I^{tar}, I^{scat}, and I^{rec} on the final, 700th iteration. Figure 2(g) shows the value of the objective function J vs. iteration number i. Figure 2(h) shows the maximum of I^{scat} vs. i. Lastly, Figure 2(i) shows the target plane peak Strehl ratio, i.e.

$$S = \frac{\max\left(I^{\text{tar}}\right)}{\max\left(I^{\text{dl}}\right)}, \tag{21}$$

where I^{dl} is the diffraction-limited target plane intensity, vs. i. The red dashed line on Fig. 2i is the estimated Strehl ratio from the wavefront fitting error variance (26), viz.,

$$S \approx \exp\left[-1.07\left(\frac{d}{r_{0,\text{sw}}}\right)^{5/3}\right]. \tag{22}$$

It is included to show the average or expected performance of the OPA. Clearly, even in the presence of turbulence and speckle, the array successfully phases on the deep (depth much greater than l_c) parabolic target.

It must be stated that, in the course of this work, array phasing performance in terms of peak Strehl ratio was inconsistent. Study of the I^{scat} images (Figure 2(b) and (e)) reveals that the rough parabolic target is composed of a relatively small number of speckle reflectors. This makes physical sense when one considers the nature of monostatic scattering from a smooth convex parabolic reflector: the main contribution to the received field comes from the specular point (under the condition that $L \gg R_T$), where the surface is normal relative to the direction of the incident ray. Indeed, this is precisely the physical consequence of using the MoSP to evaluate the Fresnel integral in (6). Adding roughness to the parabolic reflector only increases the number of specular points – the average number is related to R_T and the standard deviation of the rough surface slopes.

In simulation after simulation, the array phased on one of these specular points (hereafter termed the dominant specular point). The location of the dominant specular point was, of course, random depending on the particular rough surface instance. If the dominant specular point was located away from the centre of the array target spot, SPGD applied tilt in an attempt to steer the pattern onto the dominant specular point. Because $d, D \gg \bar{\lambda}$ in OPAs, electronic beam steering, like that used in RF phased arrays, is very inefficient resulting in a significant drop in peak Strehl ratio (27, 28). A small amount of this steering can actually be seen in Figure 2(d) and (e). Atmospheric tilt generally makes things worse by moving the target spot significantly off axis (i.e. beam wander). A tracking system in combination with a beam director could be used to ameliorate this problem. Although the final peak Strehl ratio may have been underwhelming in some instances, in every simulation, I^{rec} changed with the dithers B and SPGD successfully phased the array on the target.

4. Conclusion

In this paper, the target-based CBC of an OPA fed by a broadband MO was investigated both theoretically and in simulation. The scenario investigated here considered OPA phasing on a rough parabolic object embedded in atmospheric turbulence. Section 2 presented the theoretical analysis of the problem. The key result was a closed-form expression for the received intensity, which revealed

the physical conditions under which target-based phasing is possible. Section 3 presented and discussed simulation results of a seven element hexagonal array phasing through turbulence on a rough parabolic target. The results validated the theoretical findings and showed that target-based phasing, with an array fed by a broadband MO, is indeed possible under realistic conditions, i.e. in the presence of turbulence, speckle, and on a target whose depth or scattering features are separated by many l_c. Future work will include experimental verification of these findings.

Disclosure statement

The views expressed in this paper are those of the authors and do not reflect the official policy or position of the U.S. Air Force, the Department of Defense, or the U.S. Government.

References

(1) Brignon, A., Ed. *Coherent Laser Beam Combining*; Wiley-VCH, Weinheim, Germany, 2013.

(2) Pulford, B.N. LOCSET Phase Locking: Operation, Diagnostics, and Applications. Ph.D. Thesis, The University of New Mexico, 2011.

(3) Shay, T.M. Theory of Electronically Phased Coherent Beam Combination without a Reference Beam. *Opt. Express* 2006, *14* (25), 12188–12195.

(4) Vorontsov, M.; Weyrauch, T.; Beresnev, L.; Carhart, G.; Liu, L.; Aschenbach, K. Adaptive Array of Phase-locked Fiber Collimators: Analysis and Experimental Demonstration. *IEEE J. Sel. Top. Quantum Electron.* 2009, *15* (2), 269–280.

(5) Vorontsov, M.; Filimonov, G.; Ovchinnikov, V.; Polnau, E.; Lachinova, S.; Weyrauch, T.; Mangano, J. Comparative Efficiency Analysis of Fiber-array and Conventional Beam Director Systems in Volume Turbulence. *Appl. Opt.* 2016, *55* (15), 4170–4185.

(6) Motes, R.A.; Shakir, S.A.; Berdine, R.W. *Introduction to High-power Fiber Lasers* 2nd ed.; Directed Energy Professional Society, Albuquerque, NM, 2013.

(7) Goodno, G.D.; McNaught, S.J.; Rothenberg, J.E.; McComb, T.S.; Thielen, P.A.; Wickham, M.G.; Weber, M.E. Active Phase and Polarization Locking of a 1.4 kW Fiber Amplifier. *Opt. Lett.* 2010, *35* (10), 1542–1544.

(8) McNaught, S.J.; Thielen, P.A.; Adams, L.N.; Ho, J.G.; Johnson, A.M.; Machan, J.P.; Rothenberg, J.E.; Shih, C.C.; Shimabukuro, D.M.; Wacks, M.P.; et al. Scalable Coherent Combining of Kilowatt Fiber Amplifiers into a 2.4-kW Beam. *IEEE J. Sel. Top. Quantum Electron.* 2014, *20* (5), 174–181.

(9) Anderson, B.; Flores, A.; Holten, R.; Dajani, I. Comparison of Phase Modulation Schemes for Coherently Combined Fiber Amplifiers. *Opt. Express* 2015, *23* (21), 27046–27060.

(10) Flores, A.; Dajani, I.; Holten, R.; Ehrenreich, T.; Anderson, B. Multi-kilowatt Diffractive Coherent Combining of Pseudorandom-modulated Fiber Amplifiers. *Opt. Eng.* 2016, *55* (9), 096101.

(11) Tyler, G.A. Accommodation of Speckle in Object-based Phasing. *J. Opt. Soc. Am. A* 2012, *29* (5), 722–733.

(12) Vorontsov, M.A.; Weyrauch, T. High-power Lasers for Directed-energy Applications: Comment. *Appl. Opt.* 2016, *55* (35), 9950–9953.

(13) Tyler, G.A. 2013. An evaluation of the Impact of Laser Coherence in HiPAT Applications. Technical Report TR-1898. the Optical Sciences Company.

(14) Hyde, M.W.; Tyler, G.A. Temporal Coherence Effects on Target-based Phasing of Laser Arrays. *J. Opt. Soc. Am. A* 2016, *33* (10), 1931–1937.

(15) Hyde, M.W.; Tyler, G.A. Rosado Garcia, C. Target-in-the-loop Phasing of a Fiber Laser Array Fed by a Linewidth-broadened Master Oscillator. *Proc. SPIE* 2017, *10192*, 101920K–101920K-7.

(16) Goodman, J.W. *Introduction to Fourier Optics* 3rd ed.; Englewood, CO, Roberts & Company, 2005.

(17) Mandel, L.; Wolf, E. *Optical Coherence and Quantum Optics*; Cambridge University, New York, NY, 1995.

(18) Goodman, J.W. *Statistical Optics* 2nd ed.; Wiley, Hoboken, NJ, 2015.

(19) Nelson, W.; Sprangle, P.; Davis, C.C. Atmospheric Propagation and Combining of High-power Lasers. *Appl. Opt.* 2016, *55* (7), 1757–1764.

(20) Balanis, C.A. *Antenna Theory: Analysis and Design* 2nd ed.; Wiley, Hoboken, NJ, 1997.

(21) Voelz, D.G.; Bush, K.A.; Idell, P.S. Illumination Coherence Effects in Laser-speckle Imaging: Modeling and Experimental Demonstration. *Appl. Opt.* 1997, *36* (8), 1781–1788.

(22) Voelz, D.G. *Computational Fourier Optics: A MATLAB Tutorial*; SPIE Press, Bellingham, WA, 2011.

(23) Schmidt, J.D. *Numerical Simulation of Optical Wave Propagation with Examples in MATLAB*; SPIE Press, Bellingham, WA, 2010.

(24) Mack, C.A. Generating Random Rough Edges, Surfaces, and Volumes. *Appl. Opt.* 2013, *52* (7), 1472–1480.

(25) Goodman, J.W. *Speckle Phenomena in Optics: Theory and Applications*; Englewood, CO, Roberts & Company, 2007.

(26) Hardy, J.W. *Adaptive Optics for Astronomical Telescopes*; Oxford University, New York, NY, 1998.

(27) Spencer, M.F.; Hyde, M.W. An Investigation of Stair Mode in Optical Phased Arrays Using Tiled Apertures. *Proc. SPIE* 2012, *8520*, 852006–852006-15.

(28) Hyde, M.W.; Wyman, J.E.; Tyler, G.A. Rigorous Investigation of the Array-tilt Aberration for Hexagonal, Optical Phased Arrays. *Appl. Opt.* 2014, *53* (11), 2416–2424.